EAA Lehrstuhl für Elektrische Antriebstechnik und Aktorik
Chair of Electrical Drives and Actuators

Forschungsberichte
Elektrische Antriebstechnik und Aktorik

Hrsg.: Prof. Dr.-Ing. Dieter Gerling

Benjamin Grothmann

Online Detection and Compensation of Sensor-Faults in Electric Drives for Automotive Applications

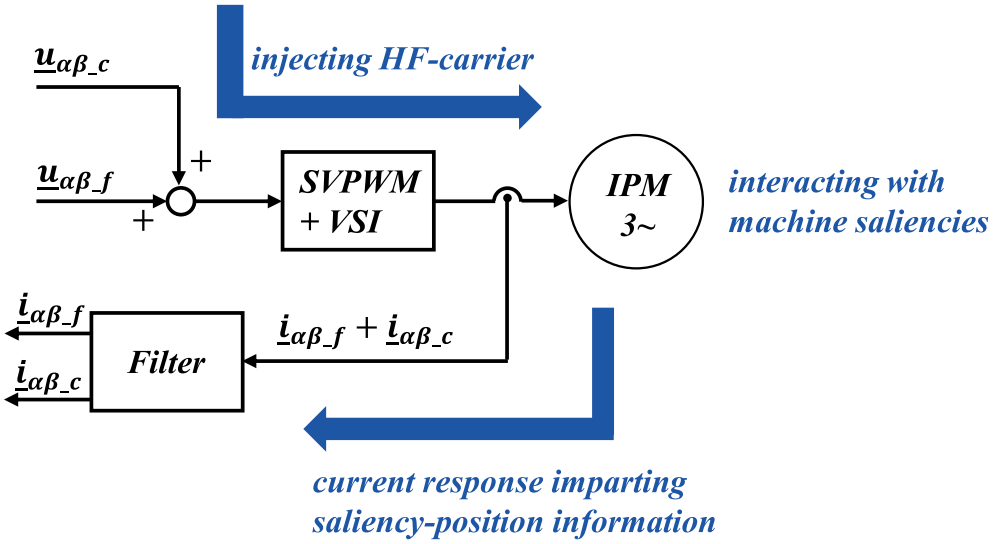

der Bundeswehr Universität München

EAA Forschungsberichte
Band 37

Online Detection and Compensation of Sensor-Faults in Electric Drives for Automotive Applications

Benjamin Grothmann

Vollständiger Abdruck der von der Fakultät für Elektro- und Informationstechnik der Universität der Bundeswehr München zur Erlangung des akademischen Grades eines

Doktor-Ingenieurs (Dr.-Ing.)

genehmigte Dissertation.

Prüfungsvorsitzender:

Prof. Dr. rer. nat. habil. Claus Hillermeier

Gutachter:

1. Prof. Dr.-Ing. Dieter Gerling

2. Prof. Robert D. Lorenz, Ph.D.

Die Dissertation wurde am 08.06.2018 bei der Universität der Bundeswehr München eingereicht und durch die Fakultät für Elektro- und Informationstechnik am 10.10.2018 angenommen. Die mündliche Prüfung fand am 29.11.2018 statt.

Forschungsberichte Elektrische Antriebstechnik und Aktorik

Band 37

Benjamin Grothmann

Online Detection and Compensation of Sensor-Faults in Electric Drives for Automotive Applications

Shaker Verlag
Aachen 2019

Bibliographic information published by the Deutsche Nationalbibliothek
The Deutsche Nationalbibliothek lists this publication in the Deutsche Nationalbibliografie; detailed bibliographic data are available in the Internet at http://dnb.d-nb.de.

Zugl.: München, Univ. der Bundeswehr, Diss., 2018

Printed in Germany.

ISBN 978-3-8440-6410-0
ISSN 1863-0707

Shaker Verlag GmbH • P.O. BOX 101818 • D-52018 Aachen
Phone: 0049/2407/9596-0 • Telefax: 0049/2407/9596-9
Internet: www.shaker.de • e-mail: info@shaker.de

In memory of Franz Wallner.
Your life and friendship will be my inspiration - forever.

Abstract

Torque production in servo drives is directly linked to current vector control and thus relying on accurate state-feedback from the sensing devices. Distortion of these signals in case of fault-occurrence in the sensors can lead to unwanted control system response. In worst-case, instability or physical damage of the system might force a shutdown of the drive. This is not tolerable especially for safety-relevant drives in automotive applications. In this thesis, methods for online detection and compensation of sensor faults for interior permanent magnet machine (IPM)-drives are developed. Position sensor outage, as well as current sensor gain faults including the case of current sensor outage, are addressed. Model-based methodologies are developed, allowing for fault-detection and fault-compensation without the requirement of auxiliary hardware alongside the already existing devices. Practical testings are conducted on a general-purpose IPM-drive representing an automotive application. Self-sensing is applied in parallel to the current regulation, using the estimated position to monitor the position transducer. Saliency-tracking self-sensing is applied for low speed-ranges, whereas back-EMF (BEMF)-based self-sensing is used for intermediate and higher speeds. Suitable transitioning between both techniques is chosen, to allow for position estimation over the complete speed operating-range. A fault-compensation framework is presented, using a weighting function to replace the faulty sensor signal with the estimated position for state-feedback, after detection of a position sensor fault. This framework is shown to achieve fast and smooth reaction to position sensor outage. Practical implementation caveats regarding self-sensing feasibility and estimation accuracy are discussed thoroughly. Based on the magnetic identification of the given drive, metrics for early assessment of self-sensing applicability are derived. Conducted testings show reliable fault-compensation for any speed operating-range. Limiting aspects identified are steep transients in commanded current and an overall physical restriciton of the given implementation to current loadings below 50 % of the specified current operating-range, at low speeds. For the compensation of current sensor gain faults, adaptive methodologies based on the deterministic response to high frequency injection (HFI) are investigated. An existing gain re-balancing scheme is optimized for fast and accurate fault-compensation. In combination with a novel direct phase gain re-balancing (DGB)-technique, the resulting gain fault-compensation framework is shown to potentially operate reliably for the complete speed operating-range. Limitations of the DGB-method regarding the calculation of reference values for the adaptive loops are discussed in detail. The DGB-technique is also proposed as suitable current sensor outage detection. Outage of one or both current sensors is then captured by enhancing the proposed compensation framework with a closed-loop observer based current vector reconstruction known from literature. Thus, the complete range of current sensor gain faults is covered. Each method for fault-compensation discussed in this thesis is assessed based on a predefined set of requirements, concluding in aspects and potentials for future optimizations.

Kurzfassung

Die Drehmomenterzeugung in Servoantrieben steht in direktem Zusammenhang mit der Regelung des Stromvektors und basiert daher auf der akuraten Bereitstellung der Ist-Werte durch die Sensorik. Abweichungen dieser Signale durch das Auftreten von Sensorfehlern können zu unerwünschten Systemantworten der Regelung führen. Im schlimmsten Falle erzwingen Instabilität oder physikalische Beschädigung des Systems ein Abschalten des Antriebs. Dies ist insbesondere für sicherheitsrelevante Antriebe in Automobilanwendungen nicht zu tolerieren. In der vorliegenden Dissertation werden Methoden zur Echtzeit-Diagnose und -Kompensation von Sensorfehlern für Antriebe mit Permanentmagnet Synchronmaschinen mit vergrabenen Magneten (IPM) entwickelt. Im Blickpunkt stehen dabei der Ausfall des Lagegebers, sowie Skalierungsfehler in den Stromsensoren inklusive Stromsensorausfall. Es werden modellbasierte Methoden entwickelt, welche die Fehlerdiagnose und Fehlerkompensation ohne Hinzunahme weiterer Hardware zu den bereits verwendeten Sensoren ermöglichen. Praktische Tests werden an einem Standard-IPM-Antrieb in Anlehnung an Automobilanwendungen durchgeführt. Eine lagegeberlose Regelung (Self-Sensing) ist parallel zur Stromregelung implementiert und der geschätzte Winkel wird zur Überwachung des Lagegebers verwendet. Für kleine Drehzahlen wird ein Anisotropie-basiertes Verfahren zur lagegeberlosen Regelung verwendet, während für mittlere bis zu hohen Drehzahlbereichen ein Verfahren basierend auf der induzierten Spannung genutzt wird. Um die Rotorlage über den gesamten Drehzahlbereich schätzen zu können wird eine geeignete Übergangsfunktion zwischen beiden Verfahren gewählt. Ein Schema zur Fehlerkompensation wird vorgestellt, welches eine Gewichtsfunktion zum Ersetzen des fehlerhaften Sensorsignals mit der geschätzten Rotorlage als Ist-Wert nach Eintreten eines Lagegeberfehlers verwendet. Es wird gezeigt, dass diese Struktur eine schnelle und sanfte Kompensation bei Ausfall des Lagegebers ermöglicht. Praktische Problemstellungen bei der Implementierung der lagegeberlosen Regelung werden detailliert diskutiert. Basierend auf der Identifikation magnetischer Systemparameter des verwendeten Antriebs werden Richtlinien zur frühen Bewertung der Umsetzbarkeit lagegeberloser Regelungen hergeleitet. Die durchgeführten Tests zeigen zuverlässige Fehlerkompensation für den kompletten Drehzahlbereich. Als limitierende Aspekte werden steile Transienten in den Strom-Sollwerten festgestellt, als auch eine physikalische Beschränkung der Anwendung auf Stromarbeitspunkte kleiner $50\ \%$ des spezifizierten Stromarbeitsbereichs für kleine Drehzahlen. Zur Kompensation von Skalierungsfehlern in der Stromsensorik werden adaptive Methoden basierend auf der deterministischen Systemantwort auf Hochfrequenz-Signalinjektion (HFI) untersucht. Eine bereits existierende Methode zum Neuabgleich von Skalierungsfehlern wird zur schnellen und akuraten Fehlerkompensation optimiert. Es wird gezeigt, dass das resultierende Konzept zur Kompensation von Skalierungsfehlern in Kombination mit einem neuartigen Verfahren zum direkten Neuabgleich der Sensorskalierungen (DGB) potentiell über dem gesamten Drehzahl-Arbeitsbereich verlässlich anwendbar ist. Limitierungen der DGB-

Methode bezüglich Berechnung von Ist-Werten ihrer adaptiven Regelschleifen werden detailliert behandelt. Die DGB-Methode wird darüber hinaus als geeignetes Verfahren zur Erkennung eines Stromsensorausfalls angedacht. Der Ausfall von einem oder beider Stromsensoren wird daraufhin durch Erweiterung des Konzepts zur Fehlerkompensation durch einen aus der Literatur bekannten Beobachter zur Rekonstruktion des Stromvektors abgefangen. Somit ist die komplette Bandbreite an Stromsensorskalierungsfehlern abgedeckt. Jedes in der vorliegenden Dissertation zur Fehlerkompensation diskutierte Verfahren wird anhand vordefinierter Anforderungskriterien bewertet, was schließlich in Aspekten und Potentialen für künftige Optimierungsansätze mündet.

Acknowledgements

First, I want to thank Prof. Dr.-Ing. Dieter Gerling for offering me this great research project, as well as the constant support and overall supervision. I am very grateful for all of his advice and motivation provided during my work. I also want to thank Prof. Robert D. Lorenz, Ph.D., for being second supervisor for this thesis and giving me the opportunity to spend a exceptionally instructive time as visiting scholar at the Wisconsin Electric Machines and Power Electronics Consortium (WEMPEC) in Madison.

At this point, many thanks go out to Marc Petit, Huthaifa Flieh, Tim Slininger, Gene Rush, Muhammad Alvi, Dan Erato and the rest of the WEMPEC-family. All the discussions and time spent together was not only fun, but also an honor and a privilege I cannot emphasize enough.
I want to thank former internship and masters-degree students at AUDI, Katharina Wiesbeck, Dennis Jagosz, Jürgen Rieblinger, Kai Taylor, Divahar Mani and Andreas Rauscher. Their talent, enthusiasm and dedication was an enrichment for the project. Further thanks also go out to Wolfgang Brandstätter, Frank Lachnit, Christine Schmidt, Christoph Raith and the rest of the AUDI R&D department for the great and always fun time.
From all of my former colleagues from the chair of electrical drives and actuators, Universität der Bundeswehr München, I want to greatly emphasize my gratitude to Michael Saur, Bastian Lehner and Niko Reiland, for their unconditional support during this thesis. In my time in Munich I was able to work together closely with Michael Saur, from which my personal development, as well as my professional career still benefit on a great scale. Special thanks also to Basti Lehner, for his always open ear, fruitful discussions and all the fun times spent together. Many, many thanks then go out to Niko Reiland, for his amazing support facing the rocky roads in our projects, including his role as a constant reminder of what day of the week it is.
Regarding my friends and supporters from Regensburg, I want to greatly thank my former professors Prof. Bernhard Hopfensperger and Prof. Dieter Seifert, for advice and support during my Masters-degree and up to this day. Thank you Andi Neumeier and Michl Forster for not only being close friends ever since we started our studies together, but also for acting as mentors during tough decisions.
I am very, very grateful for the long list of my friends from my hometown, especially Robert, Sabrina, Patrick, Tanja, Anton, Karin, Caro, Martin, Benedikt, Steffi, Manfred, Christine, Daniel and Katharina, for their support and suffering all the hard times during this project, reminding me of where my heart can always find a place to call home.

These last lines I saved for thanking my parents, Franziska and Nik. Without you, I would never be at where I am right now.

Contents

List of Figures

List of Tables

Nomenclature

List of Abbreviations

AC	alternating current
BW	bandwidth
BEMF	back electromotive force
CL	closed-loop
CO	current observer
CVC	complex vector current regulator
CVFFT	complex vector fast Fourier transform
DC	direct current
DGB	direct phase-gain re-balancing
FFT	fast Fourier transform
FSCW	fractional slot concentrated windings
HF	high frequency
HFI	high frequency injection
IPM	interior permanent magnet synchronous machine
MIMO	multiple-input multiple-output
MO	motion observer
MTPA	maximum torque per ampere
OP	operating-point
PI	proportional integral
PID	proportional integral differential
PM	permanent magnet
SDFT	sliding discrete Fourier transform
SFb	state-feedback
SGB	sequence-based gain re-balancing
SISO	single-input single-output
SNR	signal-to-noise ratio
SPM	surface mounted permanent magnet synchronous machine
SRFF	synchronous reference frame filter
SSRFF	subtraction-based synchronous reference frame filter
SVPWM	space vector pulse width modulation
TO	tracking observer
VSI	voltage source inverter

List of Symbols

General Notation

u	stator voltage
i	stator current
ψ	flux linkage
ω	angular velocity
θ	rotor position
L	inductance
j	complex number
A, B, C	three phase notation
$x_A,\ x_B,\ x_C$	three phase (ABC) quantity x
$\underline{x}_{dq} = x_d + jx_q$	complex vector x in rotary (dq) reference frame
$x_d,\ x_q$	complex components in rotary (dq) reference frame
$\underline{x}_{\alpha\beta} = x_\alpha + jx_\beta$	complex vector x in stationary ($\alpha\beta$) reference frame
$x_\alpha,\ x_\beta$	complex components in stationary ($\alpha\beta$) reference frame
X	magnitude of signal x
$\boldsymbol{x}$	scalar state vector
$\boldsymbol{X}$	scalar matrix
$\hat{x}$	estimate of x
x^*	command/reference of x
$\dot{x}$	derivative of x
x_c	carrier signal x
$x[k]$	quantity x sampled at k-th sample instant
$\boldsymbol{X}^{-1}$	matrix inverse of $\boldsymbol{X}$
$\underline{x}^\dagger$	complex conjugate of complex vector $\underline{x}$

Special Symbols

$A_1,\ A_2$	generic identifiers
$\boldsymbol{A}$	generic system matrix
$B_1,\ B_2$	generic identifiers
$\boldsymbol{B}$	generic input matrix
b	active damping controller gain
$\boldsymbol{C}$	generic output matrix
D	generic disturbance
ε	error signal
$\varepsilon_{pc},\ \varepsilon_{cp}$	error signals in SGB method created from positive sequence
$\varepsilon_{nc},\ \varepsilon_{cn}$	error signals in SGB method created from negative sequence
$\varepsilon_A,\ \varepsilon_B$	error signals in DGB method created from respective phase gain errors
$\varepsilon\underline{i}_{\alpha\beta},\ \varepsilon\underline{i}_{dq},\ \Delta\underline{i}_{dq}$	current vector deviations
e_{PM}	BEMF voltage
ϵf	set of eigenvalues

$\underline{e}_{\alpha\beta}$	BEMF voltage vector in stationary ($\alpha\beta$) reference frame
γ	relative difference saliency ratio
f_c	carrier frequency in [Hz]
f_i	generic injection frequency in [Hz]
f_r	excitation frequency in [Hz]
f_s	sampling/switching frequency in [Hz]
f_{BW}	bandwidth in [Hz]
f_{AC}	identification test signal frequency in [Hz]
G_{CL}	closed-loop transfer function
G_{dq}	transfer function of a system in dq vector notation
G_o	open-loop transfer function
G_{PI}	proportional integral controller transfer function
$\boldsymbol{G(\theta_r)}$	sensor gain matrix for current reconstruction
h	harmonic number
$i_{Ac},\ i_{Bc},\ i_{Cc}$	three phase carrier current responses to HFI
$i_{Am},\ i_{Bm}$	measured phase currents scaled by sensor gains
$i_{\hat{q}c}$	quadrature carrier current vector component in estimated dq reference frame
$\underline{i}_{\alpha\beta\_f}$	fundamental current vector in stationary ($\alpha\beta$) reference frame
$\underline{i}_{dq,AC} = i_{d,AC} + ji_{q,AC}$	alternating test signal current vector in rotary (dq) reference frame
$\underline{i}_{dq,DC} = i_{d,DC} + ji_{q,DC}$	static operating point current vector in rotary (dq) reference frame
$\underline{i}_{dq,HF}$	injection current vector in rotary (dq) reference frame
$\underline{i}_{dq\_f}$	fundamental current vector in rotary (dq) reference frame
$\underline{i}_{\alpha\beta\_c} = i_{\alpha\_c} + ji_{\beta\_c}$	carrier current response to HFI
$\underline{i}_{\alpha\beta cm} = i_{\alpha cm} + ji_{\beta cm}$	measured carrier current response to HFI scaled by sensor gains
$\underline{i}_{\alpha\beta\_cn} = i_{\alpha\_cn} + ji_{\beta\_cn}$	negative sequence carrier current response to HFI
$\underline{i}_{\alpha\beta\_cp}$	positive sequence carrier current response to HFI
$\underline{i}_n$	generic current vector associated with a negative sequence
$\underline{i}_p$	generic current vector associated with a positive sequence
$\underline{i}_{dq,M} = i_{d,M} + ji_{q,M}$	current vector in rotary (dq) reference frame for motoring operation
$\underline{i}_{dq,G} = i_{d,G} + ji_{q,G}$	current vector in rotary (dq) reference frame for generating/breaking operation
$\underline{i}^{cn}_{dqs\_cn}$	negative sequence vector isolated in its negative sequence reference frame
I_c	positive sequence carrier current vector magnitude (SPM)
I_{cn}	negative sequence carrier current vector magnitude

I_{cp}	positive sequence carrier current vector magnitude
I_{cn_cs}	negative sequence carrier current vector magnitude through of cross-saturation
I_{cns}	resulting negative sequence carrier current vector magnitude including cross-saturation
I_{cn_h}	multiple saliency vector magnitude
I_{max}	specified maximum current
J	rotor inertia
K	generic identifier
$k_A,\ k_B$	phase current sensor gains
Δk	difference gain
Σk	mean gain
$\boldsymbol{K_{AB}}$	sensor phase gain matrix
$\boldsymbol{K_{\alpha\beta}}$	sensor gain matrix transformed into stationary ($\alpha\beta$) reference frame
$K_p,\ K_P,\ K_{Pd},\ K_{Pq},\ r_o$	proportional controller gain stages
$K_i,\ K_{iA},\ K_{iB},\ K_I,\ r_{io}$	integral controller gain stages
K_{err}	weighting factor
K	active stiffness controller gain
K_M	mean error correction factor (SGB method)
K_R	relative error correction factor (SGB method)
$K_A,\ K_B$	phase error correction factors (DGB method)
$L_d,\ L_q$	apparent direct and quadrature (self-) inductance
$M_{dq},\ M_{qd}$	apparent mutual inductances
L_{dq}	unified inductance substitute
$\boldsymbol{L_{dq}}$	apparent inductance matrix in rotary (dq) reference frame
$\boldsymbol{L_{\alpha\beta}}$	apparent inductance matrix in stationary ($\alpha\beta$) reference frame
$\boldsymbol{l_{dq}}$	differential inductance matrix in rotary (dq) reference frame
$\boldsymbol{l_{\alpha\beta}}$	differential inductance matrix in stationary ($\alpha\beta$) reference frame
L_s	synchronous inductance
ΔL	difference inductance (in terms of apparent inductances)
Δl	difference inductance (in terms of differential inductances)
ΣL	average inductance (in terms of apparent inductances)
Σl	average inductance (in terms of differential inductances)
$l_{dd},\ l_{qq}$	direct and quadrature differential (self-) inductance
$l_{dq},\ l_{qd}$	differential mutual inductances
n	rotor speed
n_{max}	specified maximum rotor speed

φ_h	phase shift with respect to harmonic h
p	number of pole pairs
ψ_{PM}	rotor flux linkage
$\underline{\psi}_{\alpha\beta,BEMF}$	rotor flux linkage vector in stationary ($\alpha\beta$) reference frame
$\underline{\psi}_{dq,M} = \psi_{d,M} + j\psi_{q,M}$	flux linkage vector in rotary (dq) reference frame for motoring operation
$\underline{\psi}_{dq,G} = \psi_{d,G} + j\psi_{q,G}$	flux linkage vector in rotary (dq) reference frame for generating/breaking operation
R	ohmic resistance
r_V	virtual resistance
s	Laplace operator
t	time
$\boldsymbol{T}$	transformation matrix
T_d	disturbance torque
T_s	sample/processing time
T_{em}	electromagnetic torque
θ_c	instantaneous phase of carrier signal response
$\theta_{cmax\_A},\ \theta_{cmax\_B}$	phases of carrier signal response waveform maximums
θ_r	rotor position in electric [deg.]
$\theta_{r,meas}$	measured rotor position in electric [deg.]
θ_{rm}	rotor position in mechanical [deg.]
θ_{error}	rotor position error in electric [deg.]
$\Delta\hat{\theta}$	angular offset
ϑ	phase shift due to cross-saturation in electric [deg.]
$\boldsymbol{u}$	scalar manipulated input vector
$\underline{u}_{\alpha\beta\_c}$	complex HFI rotary voltage vector
$\boldsymbol{u_{\alpha\beta\_c}}$	scalar HFI rotary voltage vector in stationary ($\alpha\beta$) reference frame
$\boldsymbol{u_{dq\_c}}$	scalar HFI rotary voltage vector in rotary (dq) reference frame
U_c	HFI voltage magnitude
$\underline{u}_{dq,AC} = u_{d,AC} + ju_{q,AC}$	alternating test signal voltage vector in rotary (dq) reference frame
$\underline{u}_{dq,DC} = u_{d,DC} + ju_{q,DC}$	static operating point voltage vector in rotary (dq) reference frame
$\underline{u}_{dq,M} = u_{d,M} + ju_{q,M}$	current vector in rotary (dq) reference frame for motoring operation
$\underline{u}_{dq,G} = u_{d,G} + ju_{q,G}$	voltage vector in rotary (dq) reference frame for generating/breaking operation
$\underline{V}_{\alpha\beta}$	generic vector in stationary ($\alpha\beta$) reference frame
v_i	generic injection voltage
ω_r	angular rotor velocity in electric [rad/s]
$\bar{\omega}_r$	average angular rotor velocity in electric [rad/s]
ω_{rm}	angular rotor velocity in mechanical [rad/s]

ω_{rmL}	filtered angular rotor velocity in mechanical [rad/s]
ω_{rmR}	regular angular rotor velocity in mechanical [rad/s]
ω_c	carrier frequency in electric [rad/s]
ω_n	negative sequence angular frequency in electric [rad/s]
ω_p	positive sequence angular frequency in electric [rad/s]
ω^*	desired bandwidth in [rad/s]
ω_{BW}	bandwidth in [rad/s]
ω_H	high pass filter bandwidth in [rad/s]
ω_L	low pass filter bandwidth in [rad/s]
$\boldsymbol{x_0}$	initial condition state vector
ξ	anisotropy ratio
$\boldsymbol{y}$	output vector
χ	generic saliency ratio